

Article

Weak Fault Feature Extraction Scheme for Intershaft Bearings Based on Linear Prediction and Order Tracking in the Rotation Speed Difference Domain

Zhinong Jiang, Minghui Hu , Kun Feng * and Ya He

College of Mechanical and Electrical Engineering, Beijing University of Chemical Technology, Chao Yang District, Beijing 100029, China; jiangzhinong@263.net (Z.J.); humh2008@163.com (M.H.); heya1301@163.com (Y.H.)

* Correspondence: kunfengphd@163.com; Tel.: +86-10-6441-1076

Received: 7 August 2017; Accepted: 10 September 2017; Published: 12 September 2017

Abstract: Because both the inner and outer rings rotate, the intershaft bearings used in gas turbines do not have fixed bearing housings. As a result, the vibration of intershaft bearings cannot be measured directly. Therefore, a vibration signal can only be collected through indirect measurement. First, it must be transferred to adjacent bearings through the shafting. Then, it should be transferred by the elastic supports and complex structure of the thin-walled strut. The vibration signal is severely weakened during transmission under the influences of the transfer path. In the meantime, in the vibration of other components, a huge amount of noise is produced by the air flow, and the variable speeds of the inner and outer rings of the intershaft bearings make it harder to analyze the signal. Hence, it is very difficult to extract the vibration fault features of intershaft bearings. To deal with the variable speed of dual rotors, as well as the weak signal, a fault feature extraction scheme for the weak fault signals of intershaft bearings is proposed in this paper. This scheme is based on linear prediction, spectral kurtosis, and order tracking in the rotation speed difference domain. First, a prewhitening process, based on linear prediction, is applied to the fault signal of the intershaft bearings to eliminate the stationary component. Thus, the remaining components, including the impulse signal of faulty bearings and nonstationary noise, can retain the features of the vibrational bearings, in addition to reducing the noise. Second, the optimal center frequency and bandwidth of the band-pass filter, applied to resonant demodulation, are selected by spectral kurtosis. Subsequently, the enveloped signal containing the features of the faults found in the intershaft bearings is obtained by resonance demodulation. The quasi-stationary signal in the angle domain is acquired by the even angle resampling of the nonstationary envelope signal, as a result of the variable speed. The final order spectrum is obtained through a Fourier transform. Fault diagnosis can be conducted for the intershaft bearings by comparing this spectrum with the feature order of the bearing fault. Experiments were conducted to verify the validity of the proposed scheme.

Keywords: fault diagnosis; intershaft bearing; weak fault feature extraction; rotation speed difference domain; linear prediction; order tracking

1. Introduction

Intershaft bearings, a type of rolling bearing, differ from traditional rolling bearings because both the inner and outer rings rotate. To obtain a compact structure, intershaft bearings are widely used in dual-rotor equipment where they play a significant role such as in gas turbines. Additionally, their functional reliability directly affects the life and safety of the equipment. The gas turbine study in this paper is aimed at gas turbines which have intershaft bearings without considering application situations. Intershaft bearings are installed close to the combustion chamber, so the

operating temperatures are very high, and large bearing clearances are designed for operating at such temperatures. Faults occur frequently in intershaft bearings because of the above reasons and the high rotational speeds. Moreover, their variable load makes their working conditions even worse. When compared with the faults in other types of bearings, faults in an intershaft bearing lead to greater damage and economic losses [1]. In order to prevent serious faults in dual-rotor equipment, it is very necessary to study the condition monitoring and fault diagnosis of intershaft bearings.

Researches on fault diagnosis for rotating machinery mainly focus on dynamic analysis and signal processing. For the former, dynamic analysis is used for recognizing and predicting a fault. A method based on dynamics and probability for calculating failure probability was investigated by de Lacalle [2]. Then, Urbikain et al. proposed semidiscretization methods instead of time domain analysis in vibration prediction. They proved that Chebyshev or homotopy can be useful to solve the basic equation more efficiently in dynamic analysis [3,4]. However, this paper focuses on the latter one.

Vibration analysis is a widely used method for rolling-element bearing (REB) condition monitoring and fault diagnosis, and the corresponding vibration signal processing methods are constantly being improved. With a fixed bearing housing, a traditional REB installed in a piece of equipment with a single rotor has an outer ring connected to the solid bearing housing. In this case, the vibration signal can be measured in the bearing housing, which is directly linked to the REB with a single rotor. Naturally, the fault features can be extracted effectively using the existing processing methods.

However, as for the intershaft bearings in dual-rotor equipment (as shown in Figure 1), fault diagnosis has several technical challenges as compared with traditional REBs. (1) As both the inner and outer rings of intershaft bearings rotate, no positions for direct measurements of vibration can be selected. The vibration must be indirectly measured, while traditional vibration of REBs can be directly measured because the outer ring is fixed; (2) As the red dotted line shown in Figure 1, elastic supports and a variety of thin-wall struts are included in the transfer path of the indirectly measured signal, so the weak signal of the intershaft bearings is buried in strong vibration and interference; (3) The inner and outer rings of the intershaft bearing rotate at different high speeds, thus the fault feature is relevant to two different and varied rotating speeds. However, as for traditional bearings, the fault feature is relevant to one rotating speed.

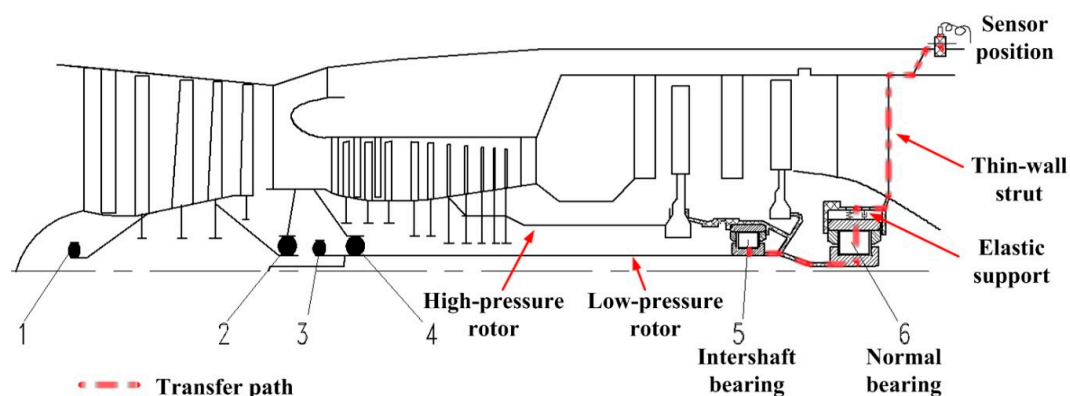


Figure 1. Schematic diagram of a gas turbine support structure.

One of the most common methods for analyzing the vibration signals of REBs is resonance demodulation, which is based on envelope analysis. However, because it is difficult to extract fault features directly from vibration signals through envelope analysis, it is necessary to filter the signal before analyzing it. This method is known as resonance demodulation. In 1974, Darlow and Badgley [5] applied resonance demodulation to fault diagnosis of bearings for the first time, achieving good results. However, this extraction method for fault features is mainly applicable to signals mixed with a small amount of noise. In addition, frequency-smear problems arise when the traditional envelope analysis method is utilized for nonstationary vibration signals that emerge as a result of speed fluctuations.

A large amount of research has been conducted by several experts on the noise reduction and filtering of the fault signals occurring in REBs. As a result of these efforts, wavelet de-noising and filtering based on spectral kurtosis (SK) have become known as reliable methods. Wavelet de-noising, which is suitable for nonstationary signals, was used by Cui et al. [6] to de-noise bearing signals and facilitate the extraction of the features of bearing faults. A synchronous averaging method in the angular domain, based on wavelet de-noising, was proposed by Mishra et al. [7] to analyze the fault signals of REBs operating at variable speeds, with a huge amount of noise. This method effectively lowers the noise levels, resolving the frequency-smear problems that occur when the traditional Fourier transform is applied to analyzing nonstationary signals. How to choose filter parameters has remained a controversial issue in academic circles for a long time. Fortunately, SK was proposed to resolve this issue. This method was primarily proposed by Dwyer [8], whose main goal was to compute the kurtosis of each spectral line and find a nonstationary signal to determine the optimal center frequency and bandwidth. Antoni [9–11] studied when and in what situations that SK can be applied to diagnosing equipment faults, and introduced the official definition of SK and the fast kurtogram algorithm. This method has provided significant benefits for the diagnosis of equipment faults. The utilization of SK in fault diagnosis of bearings has also been improved. The autoregressive (AR) model has been applied to processing the signal before SK is used. Meanwhile, a complex Morlet wavelet has been adopted to decompose the signal. After the optimal filter parameters are determined, the accurate fault characteristic frequency (FCF) of a bearing will be obtained in the envelope spectrum [12]. In recent years, SK has been improved and applied to the fault diagnosis for the bearings and gears used in rotating machinery. Adaptive spectral kurtosis (ASK) was proposed to identify multiple faults in bearings and successfully extracted the features of multiple faults buried by strong noise components [13]. In 2016, Wang et al. [14] summarized the researches on the application of SK to fault diagnosis and prediction for rotating machinery after the method had been proposed in 1983. At the same time, experts suggested that SK had reached its full potential in areas such as operational modal analysis and fault diagnosis of electronic machinery. Therefore, SK-based filtering was adopted in this study. In addition, many other types of fault diagnosis methods for REBs have been studied. Tian X. et al. proposed a modulation signal bi-spectrum based method in determining optimal bands for bearing diagnosis when the signal is very noisy [15]. Zhang et al. proposed a method of rolling bearings fault diagnosis based on variational mode decomposition (VMD). They mainly dealt with the traditional REBs used in the multistage centrifugal pump, and confirmed that the method can extract the fault feature effectively [16].

An order tracking method for rotating machinery was initially proposed in 1990 by R. Potter [17]. Then, a computed order tracking method was proposed in 1997 by Fyfe and Munck [18] to deal with the problems that occurred when feature extraction was conducted on rolling bearings operating at variable speeds. This method can also be used to achieve a stationary signal in the angular domain rather than a nonstationary signal in the time domain. Borghesani et al. [19] applied envelope analysis, based on order tracking, to a nonstationary signal and introduced prewhitening to improve the signal-to-noise ratio. Consequently, the benefit of applying this method to fault feature extraction for rolling bearings has been well proven. Randall et al. proposed a semi-automated bearing diagnostic procedure, which combined order tracking with linear prediction, minimum entropy deconvolution, spectral kurtosis, and envelope analysis [20,21]. However, this method mainly dealt with traditional REBs at slightly fluctuant operating speed, without considering two different rotating speeds and sharp changes in speeds. Liu et al. [22] combined SK and order tracking with envelope demodulation to effectively diagnose the faults in rolling bearings of rotating machinery working at variable speeds. However, this method is mainly suitable for equipment with a single rotor and can be utilized when the vibration signal is directly measured at the housing of the faulty bearing.

At present, the majority of the researches on extracting the fault features of REBs focus on traditional REBs used with a single rotor and fixed housing. However, it remains difficult to extract the fault features of intershaft bearings using these methods.

This study considers inner and outer rings with variable rotation speeds. It proposes an order tracking method in the rotating-speed difference domain, which differs from traditional order tracking. Meanwhile, prewhitening based on linear prediction and SK is also adopted to extract the weak fault features of the intershaft bearing. Based on the above approaches for extracting the weak fault features of intershaft bearings, a scheme composed of linear prediction, SK, and order tracking in the rotating-speed difference domain is proposed. The fault diagnosis of intershaft bearings can effectively be performed using this proposed scheme when equipment with dual rotors operates at variable speeds.

The structure of this paper is as follows. Section 2 explains the computing method for calculating the FCF of intershaft bearings and the prewhitening processing method based on linear prediction. The theoretical bases of SK and order tracking are also presented. Section 3 describes the proposed scheme, which adopts linear prediction, SK, and order tracking in the rotating-speed difference domain to extract the weak fault features of the intershaft bearings. Moreover, the application of this scheme is discussed in this section. The simulated and experimental signals of intershaft bearing faults are analyzed in Sections 4 and 5, respectively, confirming the effectiveness and value of the methods discussed in this paper. Section 6 presents the conclusions of the study.

2. Basic Theory

2.1. FCF of Intershaft Bearing

When the working surface of a bearing has defects, these defects will collide with its contact component and generate impact vibration, causing changes in the different components of the bearing. In practice, the impact vibration frequency is known as the FCF. When bearing components have defects, such a vibration frequency will be evident, making it possible to determine whether bearing parts suffer from faults. Equations (1)–(3) are the FCF equations for a traditional bearing's inner race, outer race, and rolling element, respectively [23]. The traditional bearing mentioned here refers to a bearing with a fixed outer ring.

$$\text{Ball Pass Frequency on Inner ring}(BPFI) = \frac{1}{2}Zf_r \left(1 + \frac{d}{D} \cos(\alpha)\right) \quad (1)$$

$$\text{Ball Pass Frequency on Outer Ring}(BPFO) = \frac{1}{2}Zf_r \left(1 - \frac{d}{D} \cos(\alpha)\right) \quad (2)$$

$$\text{Ball Spin Frequency}(BSF) = \frac{f_r D}{2d} \left(1 - \left(\frac{d}{D} \cos(\alpha)\right)^2\right) \quad (3)$$

where f_i (Hz) represents the rotating frequency of the bearing's inner race, d (mm) is the diameter of the rolling element, D (mm) is the pitch circle diameter of the REB, and α is the contact angle.

Unlike traditional bearings, an intershaft bearing's inner and outer rings both rotate. Therefore, the FCF equations for a traditional bearing cannot be directly applied to intershaft bearings. Assuming that a sensor is installed in the outer ring (in fact it is impossible), namely, the sensor rotates synchronously with the outer ring. As for the sensor, the outer ring is relatively motionless because it is in the relative coordinate system. In this coordinate system, the outer ring is motionless and the rotating frequency of the inner ring is $|f_0 - f_i|$. This coordinate system is defined as rotating speed difference domain. In this domain, Equations (1)–(3) can be applied to intershaft bearings. No matter in which coordinate system, the FCFs are constant. Therefore, the FCF equations for intershaft bearings with inner and outer rings have the same rotating directions as shown in Equations (4)–(6)

$$BPFI = \frac{1}{2}Z|f_0 - f_i| \left(1 + \frac{d}{D} \cos(\alpha)\right) \quad (4)$$

$$BPFO = \frac{1}{2}Z|f_0 - f_i| \left(1 - \frac{d}{D} \cos(\alpha)\right) \tag{5}$$

$$BSF = \frac{1}{2}|f_0 - f_i| \frac{D}{d} \left(1 - \left(\frac{d}{D} \cos(\alpha)\right)^2\right) \tag{6}$$

where f_0 (Hz) represents the rotating frequency of the bearing’s outer race, and the other parameters have the same meanings as defined for Equations (1)–(3).

There are two main frequencies that greatly influence the envelope demodulation analysis of bearing fault diagnosis: (1) the bearing FCF, which is associated with the rotating speed; and (2) the carrier frequency, which determines the demodulation bandwidth. This is irrelevant to the rotating speed but relevant to the resonance frequency of the bearing components and signal transmission path.

2.2. Prewhitening Processing by Linear Prediction

In linear prediction, the AR model is applied to predict $x(n)$ at time n according to the P data $\{x(n - p), x(n - p + 1), \dots, x(n - 1)\}$ obtained before time n [24]. The AR model can be written as

$$\hat{x}(n) = -\sum_{k=1}^p a_k x(n - k) \tag{7}$$

where $\hat{x}(n)$ represents the predicted value.

The actual signal value is the sum of the predicted value $\hat{x}(n)$ and the value of residual $e(n)$, then

$$e(n) = x(n) - \hat{x}(n) = x(n) + \sum_{k=1}^p a_k x(n - k) \tag{8}$$

Further expanding Equation (8),

$$e(n) = 1 \cdot x(n) + a_1 x(n - 1) + a_2 x(n - 2) + \dots + a_p x(n - p) \tag{9}$$

It can be seen that filter $a(n)$, constituted by $1, a_1, a_2, \dots, a_p$, can convert $x(n)$ into $e(n)$. As for stationary signals, the residual signal is mainly white noise. As for nonstationary signals, the residual signal consists of noisy signals and nonstationary components of the original signal [25]. Therefore, $a(n)$ is known as a whitening filter, as shown in Figure 2.

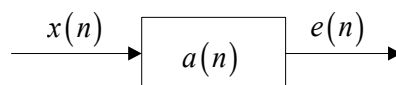


Figure 2. Whitening filter.

The parameters a_1, a_2, \dots, a_p in Equation (9) are unknown and can be obtained using the Yule-Walker equation [26].

Under variable speeds, fault signals of an intershaft bearing are nonperiodic, and the impacts are weakening. Therefore, the whitening filter can remove the stationary components from the signals and retain more fault information in $e(n)$.

As is shown in Figure 2, output $e(n)$ is the result after the input signal $x(n)$ has been processed by the whitening filter $a(n)$, and the processing procedure has undergone convolution. Convolution must be done after the $x(n)$ have been stored in the computer memory in general. In terms of practical signals, $x(n)$ might be very long. If convolution is performed after $x(n)$ is stored, there will be two problems. First, too much computer memory is required. Second, it takes too long to input $x(n)$ and

the “real-time processing” of the signal cannot be realized. To solve this problem, we divide $x(n)$ into smaller sections, each one with a length of L ; then

$$x_i(n), i = 1, 2, \dots, N/L$$

where N represents the total signal length. After the convolution of $x_i(n)$ and $a(n)$, $e_i(n)$ can be obtained. Then, the complete output $e(n)$ will be known when $e_i(n)$ sequences have been done end-to-end according to a certain rule [26].

Assume that $x(n)$ is a sequence of M points, and $a(n)$ is a sequence of L points. After their convolution, $e(n)$ will be a sequence of $(M + L - 1)$ points. The convolution of long sequences in this paper is realized using a discrete Fourier transform (DFT), as shown in Equation (10):

$$e(n) = x(n) * a(n) = IDFT[X(k)A(k)] = IDFT[E(k)] \tag{10}$$

The above derivation and algorithm are realized after the first $p + 1$ autocorrelation functions of $x(n)$ are known. In practical applications, the autocorrelation function of $x(n)$ cannot be known in most cases; only the data of N points can be obtained, which are $x_N(n), n = 0, 1, \dots, N - 1$. Therefore, the specific design and function of the whitening filter can be obtained as follows:

- (1) The $\hat{r}_x(m)$ and autocorrelation function of $x(n)$ can be estimated when $x_N(n)$ is known, $m = 0, 1, \dots, p$.
- (2) After the solution to the Yule-Walker equation with $\hat{r}_x(m)$ is obtained, the estimated values of the whitening filter parameters are known: $\hat{a}(1), \hat{a}(2), \dots, \hat{a}(p)$.
- (3) $a(0) = 1, a(n) = [a(0) a(1) \dots a(p)]$. The residual signal $e(n)$ can be obtained after the linear convolution of $x(n)$ and $a(n)$ has been performed using the DFT.

2.3. Spectral Kurtosis

Kurtosis refers to a wave peak statistic that describes the distribution characteristics of vibration signals. Because it is sensitive to impact signals, it can be used to diagnose the faults of damaged surfaces, and is effective in the early detection of faults. As global characteristics, kurtosis values are affected by weak fault features and the interference of noise or other unknown components in the signal. SK, which was proposed by Dwyer [8], represents the kurtosis of the original data at a specific frequency. It can be calculated as follows:

$$K(f) = \frac{E[|X(t, f)|^4]}{\{E[|X(t, f)|^2]\}^2} - 2 \tag{11}$$

where $|\cdot|$ and $E[\cdot]$ represent the absolute value and expectation, respectively, and $X(t, f)$ refers to the complex envelope of signal $x(t)$ in frequency f . $X(t, f)$ can be computed using the short-time Fourier transform (STFT) or fast computation of SK [24]. Based on the STFT, nonstationary signals will be processed as local stationary signals; thus, it is not applicable to impact signals. When an inappropriate frequency resolution Δf is chosen, the computation of SK by STFT will be affected. Therefore, this paper adopts the latter for computation.

By building a series of band-pass filters with a pyramid algorithm, the SK in each frequency band inside the plane composed of f and Δf can be obtained through fast computation of SK [11]. Thus, the maximum value of SK and the optimal frequency band can be determined. The computation steps are as follows:

- (1) Design a low-pass filter $h(n)$ with a cut-off frequency of $1/8$, and set up a quasi-analytical filter based on $h(n)$. The normalized analysis frequency band of the quasi-analytical low-pass filter

$h_0(n)$ is $[0,1/4]$. Correspondingly, the normalized analysis frequency band of the quasi-analytical high-pass filter $h_1(n)$ is $[1/4,1/2]$. The equations are as follows:

$$\begin{cases} h_0(n) = h(n) \cdot e^{j\pi n/4} \\ h_1(n) = h(n) \cdot e^{j3\pi/4} \end{cases} \quad (12)$$

- (2) Apply $h_0(n)$ and $h_1(n)$ to filtering the signal. Then, the results after being filtered are reducing, sampled twice to ensure that each layer resolved by the filter is the same as the original data in terms of length. According to Equation (11), the original signal will be resolved with the k layer. The decomposition algorithm can be realized as follows:

$$\begin{cases} c_{k+1}^{2i}(m) = h_0(n) * c_k^i(2m) \\ c_{k+1}^{2i+1}(m) = h_1(n) * c_k^i(2m) \end{cases} \quad (13)$$

The output $c_k^i(n)$ will be obtained after the original signal is filtered through the i th filter at the k th layer, and the value of i ranges from 0 to $2^k - 1$. $c_k^i(n)$ can also be regarded as the complex envelope of the band-pass signal whose center frequency is $f_i = (i + 2^{-1})2^{k-1}$ and bandwidth is $\Delta f_k = 2^{k-1}$. To improve the decomposition accuracy and avoid similarity between the SK values of frequency bands $[0,1/4]$ and $[1/4,1/2]$, additional decompositions of $[0,1/6]$, $[1/6,1/3]$, and $[1/3,1/2]$ are conducted at each layer, and three signals are obtained. The principle here is the same as that of the two decomposition signals previously discussed.

- (3) Calculate the kurtosis of each output signal $c_k^i(n)$ and obtain the kurtosis of the practical signal according to Equation (14):

$$K(f_i, \Delta f_k) = \frac{E\langle |c_k^i|^4 \rangle}{\{E\langle |c_k^i(n)|^2 \rangle\}^2} - 2 \quad (14)$$

Perform quantization of the kurtosis with color and draw a fast spectral kurtogram.

- (4) The optimal center frequency f_c , bandwidth B_w , and envelope signal $c_0(n)$ can be obtained when $K(f_i, \Delta f_k)$ is the maximum:

$$[f_c, B_w, c_0(n)] = \operatorname{argmax}\{K(f_i, \Delta f_k)\} \quad (15)$$

where *argmax* represents the corresponding independent variable parameters when K is the maximum, that is, the *argmax* corresponds to the optimal center frequency f_c , bandwidth B_w , and complex envelope signal $c_0(n)$.

2.4. Order Tracking

The order refers to the number of vibrations in each rotation of the shaft. Thus, the order is irrelevant to the rotating speed. The definition of order is shown in Equation (16):

$$O = \frac{60f}{n} \quad (16)$$

where O represents the order, n (r/min) denotes the rotating speed of the shaft, and f (Hz) represents the vibration frequency.

The key point of order analysis is even angle sampling, while the key point of even angle sampling is to acquire sampling time. After the sampling time is known, stationary signals in the angle domain will be obtained by interpolating and fitting the original signal [18].

As shown in Equations (4)–(6), the FCFs of intershaft bearings are proportional to $|f_0 - f_i|$. Therefore, an order tracking method in the speed difference domain is required for feature extraction of the intershaft bearing’s faults. This order tracking method is different from traditional order tracking methods because traditional ones are based on one speed which can be measured directly. To extract the fault features of intershaft bearing, vibration data needs to be order-tracked according to the difference of the two rotational speeds. The difference and its key phasor pulse cannot be directly measured. Therefore, the even angle sampling time must be selected on the basis of the trend of the rotational speed difference. The details of the procedures are as follows.

- (1) Resampling of original vibration: A polyphasic finite impulse response filter is adopted to upsample the frequency. As a result, frequency aliasing in even angle sampling can be avoided [27].

Resampling, which is to raise the sampling frequency, is obtained through interpolation on the original signal. As shown in Figure 3, $v(n)$ can be obtained by raising the sampling frequency of the original signal $x(n)$ to its L times; in other words, $L - 1$ zeros are inserted between the adjacent elements of $x(n)$. Then, the output $y(n)$ with interpolation is obtained by designing low-pass filter $h(n)$ to the process $v(n)$.

$$v(n) = \begin{cases} x(n/L) & n = 0, \pm L, \pm 2L, \dots \\ 0 & \text{others} \end{cases} \quad (17)$$

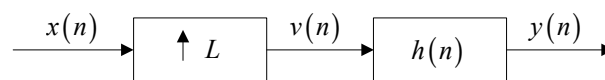


Figure 3. Flowchart of interpolation filtering.

- (2) Acquiring the even angle sequence: The corresponding rotation angle at each sampling point is obtained according to the trend of the rotational speed difference. Then, the minimum and maximum angles are determined to obtain the even angle sequence on the basis of the principle that the sampling number per revolution is twice the maximum order to be analyzed (sampling when the shaft passes the even angle point) [28].

Assuming that the original sampling interval is Δt and the rotational speed difference of the k th sampling point i is v_i , then the computation equation for the corresponding rotation angle is

$$\theta_i = 2\pi\Delta t \times \frac{v_i}{60} \quad (18)$$

The sampling time is $t_i = k\Delta t$ and the shaft rotation angle at the moment is

$$\theta_{t_i} = \sum_{i=1}^k \theta_i \quad (19)$$

Therefore, the sampling point of the even angle during $t_1 - t_i$ is as follows:

$$N_i = 2 \times MaxOrder \times \frac{(\theta_{t_i} - \theta_{t_1})}{2\pi} \quad (20)$$

where $MaxOrder$ is the maximum order to be analyzed. According to the sampling theorem of even angle sampling, the minimum sampling number per revolution is $2 \times MaxOrder$, the sampling frequency in the angle domain. According to the Shannon sampling theorem, $MaxOrder$ can be written as

$$2 \times MaxOrder \times \frac{n_{max}}{60} \leq f_s \quad (21)$$

where n_{\max} denotes the maximum speed difference within the sampling work, and f_s is the sampling frequency of the original signal. Therefore, the even angle sequence θ_n is written as

$$\theta_n = \frac{\theta_{t_i}}{N_i} \tag{22}$$

- (3) Two interpolations: Interpolation can be conducted on the basis of the corresponding relations of two groups of data, and the value of the nonsampled data can also be obtained.

Piecewise linear interpolation has been adopted in this paper, which holds that two sampling points conform to the linear function $y = ax + b$. Therefore, with dependent or independent variables between two points, another variable can be obtained. In Figure 4, the red point refers to a sampling point, whose time interval is Δt . The sampling time of even angle T_n can be obtained by interpolating between the sampling points with an even angle interval $\Delta\theta$.

Regardless of the rotating speed, the stationary signal in the speed difference domain will be obtained after the resampled signal is interpolated and fitted through the sampling time of even angle. Figure 5 shows the flowchart of the even angle resampling according to the speed difference trend.

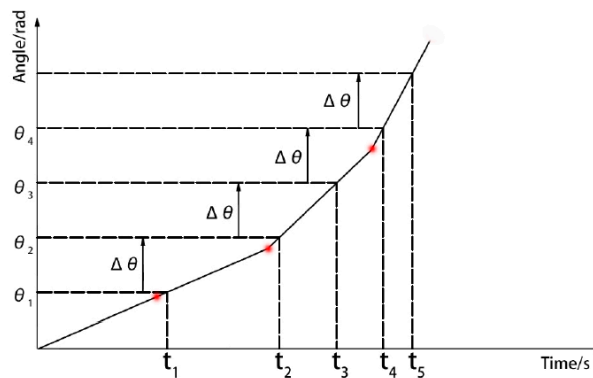


Figure 4. Even angle sampling time after interpolation.

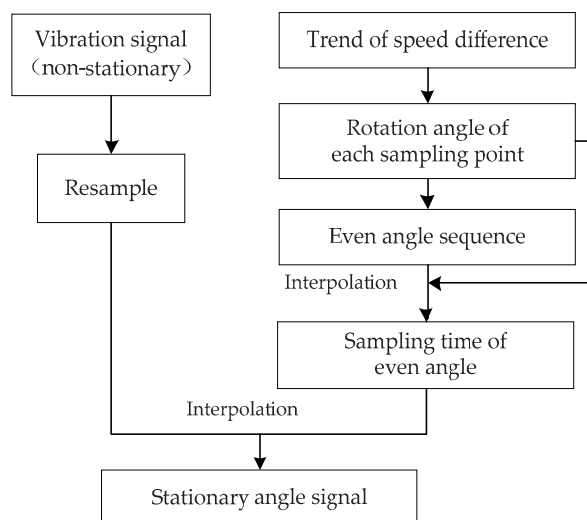


Figure 5. Flowchart of even angle resampling.

3. Proposed Method

A type of intershaft bearing whose inner and outer rings have the same direction of rotation was studied. Figure 6 explains the methods and principles of weak fault feature extraction for an intershaft

bearing, based on linear prediction, SK, and order tracking in the speed difference domain. The steps of this method are as follows:

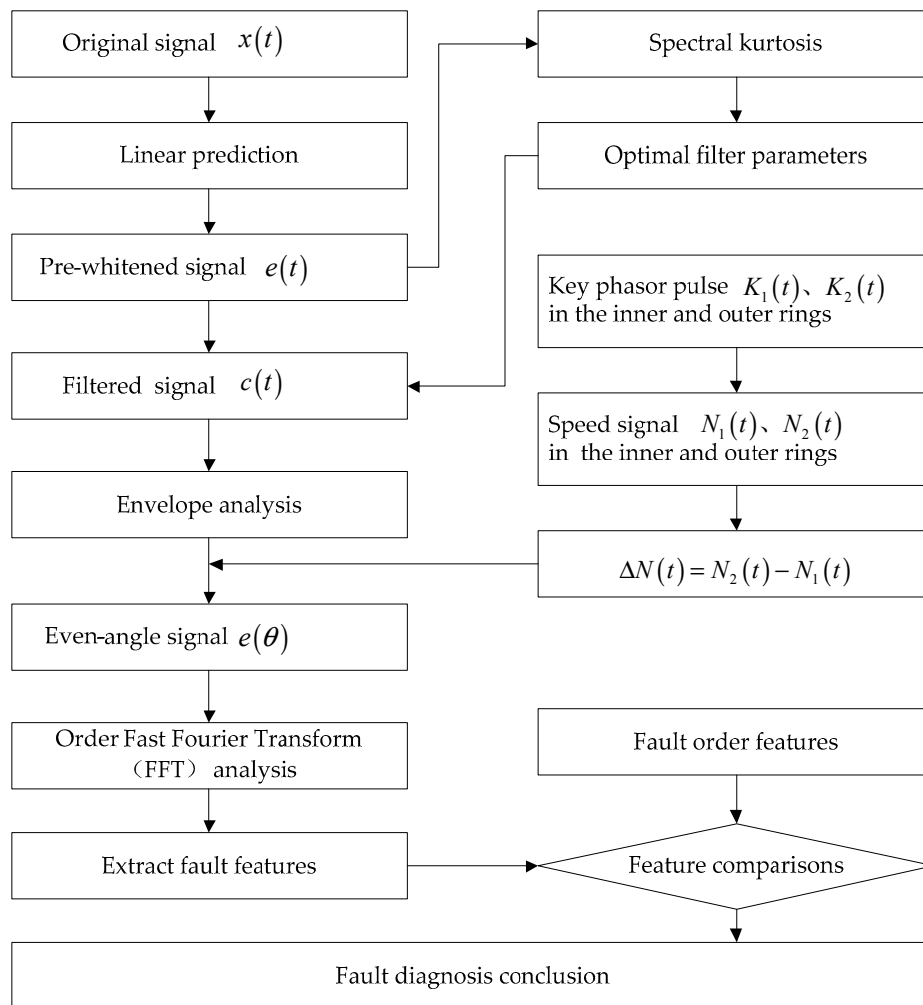


Figure 6. Schematic of proposed method.

- (1) Prewhitening through linear prediction. First, the filter parameter $a(n)$ is determined by the whitening filter, which is designed for the original vibration signal $x(n)$ of the intershaft bearing according to the Yule-Walker equation. Next, the linear convolution is found by applying Equation (10). Then, the residual signal $e(n)$ is achieved, which satisfies the prewhitening expectations.
- (2) Envelope extraction based on SK. First, signal $e(n)$, which has been prewhitened previously, is decomposed according to Equation (13) to obtain the complex envelope signals $c_k^i(n)$, which have different center frequencies and bandwidths. Then, the SK of each complex envelope signal is evaluated using Equation (14). Finally, the optimal envelope center frequency f_c , bandwidth B_w , and optimized complex envelope signal $c_o(n)$ are determined according to Equation (15). Hence, the adaptive extraction of the envelope signal is completed, extracting the weak signals of the bearing from strong noises.
- (3) Even angle resampling in the speed difference domain. Speed trends, like $N_1(t)$ and $N_2(t)$, can be calculated using the key pulses of the dual rotors, including $K_1(t)$ and $K_2(t)$. Then, the speed difference series $\Delta N(t)$ can be evaluated when the difference between the two speed trends is known. The even angle resample can be realized using $\Delta N(t)$.

In even angle resampling, the prerequisite is to know the sampling time of the even angle. This can be evaluated with the following steps. First, angle θ_i can be obtained using Equations (18) and (19) based on the k th sampling point i , as well as the shaft rotating angle θ_{t_i} at time t_i Equations. Next, the even angle series θ_n can be evaluated from Equations (20) and (22). Then, the sampling time of the even angle can be determined through piecewise linear interpolation, which can be evaluated using the following equation:

$$T_n = \frac{\theta_n - b_i}{a_i} \tag{23}$$

where a_i and b_i are the fitting coefficients of the linear function at the i th and the $i + 1$ th sample points, respectively. Finally, $c_o(T_n)$, the stationary signal in the angle domain, can be obtained after the resampled vibration signals are interpolated and fitted by the sampling time of the even angle.

- (4) Analysis of fault features. The order spectrum can be determined after the even angle signal $c_o(T_n)$ is processed by the fast Fourier transform. The fault diagnosis results can be obtained after the order spectrum analysis and calculation of the FCF order of the intershaft bearings according to Equations (4)–(6).

4. Simulation

To verify the proposed method, the fault signal for the inner ring of an intershaft bearing operating at variable speeds was simulated using MATLAB. The simulations are as follows [29–31]:

t is regarded as the equal time interval series of $L = 32,768$, and the interval is $1/f_s$, where $f_s = 51.2$ kHz is the sampling frequency;

$$f_o = \frac{3}{2}at + \frac{5}{4}b \tag{24}$$

$$f_i = \frac{1}{2}at + \frac{1}{4}b \tag{25}$$

$$f_r = at + b \tag{26}$$

where f_o denotes rotational frequency of the outer race, f_i represents rotational frequency of the inner race, f_r denotes the frequency difference of f_o and f_i , which has linear relationship with time; a represents the change rate of rotational frequency; and b represents the basic frequency. The model of a reference vibration signal can be obtained through Equation (26). These processes are shown in Equation (27). The frequency of x_n varies linearly with frequency difference f_r

$$x_n = \sin(2\pi n f_r t) \tag{27}$$

where $n = 5.3$ denotes the FCF order of the bearings. t_j is the time when the value of x_n reaches its maximum in every period, $j = 1, 2 \dots \dots N$.

$$A = \cos(2\pi f_i t + \omega_{\varphi 1}) + 3 \tag{28}$$

$$h(t) = e^{(-Bt_0)} \cdot \cos(2\pi f_n t_0 + \omega_{\varphi 2}) \tag{29}$$

$$x_{bi} = A \cdot \sum_{j=1}^N h(t - t_j) \tag{30}$$

Equation (30) is the simulated signal of the intershaft bearing’s inner fault, which can be obtained by utilizing Equations (28) and (29). In Equation (29), coefficient B denotes the decay rate of the decline exponential function, and $f_n = 4$ kHz represents the natural frequency of the system. $\omega_{\varphi 1}$ and $\omega_{\varphi 2}$ represent the signal phases and are 45° and 30° , respectively. Equation (28) is the amplitude modulator which is caused by the rotational speed of the inner ring.

$$x_O = 0.2 \cos(2\pi f_O t + \pi/3) \tag{31}$$

$$x_i = 0.1 \cos(2\pi f_i t + \pi/6) \tag{32}$$

$$x = x_{bi} + x_O + x_i \tag{33}$$

where x_O represents the vibration signal generated by slight unbalance of the outer rotor, x_i denotes the vibration signal generated by slight unbalance of the inner rotor, x is the fault simulation signals of intershaft bearing operating at time-varying speeds.

To prove the validity of using the prewhitening algorithm based on linear prediction to extract the fault features of the intershaft bearing, the signal obtained from the above simulation (without noise) are utilized, as shown in Figure 7. Results are shown in Figure 8. The kurtosis value has been improved from 4.8 to 96.5 as a result of being prewhitened. This shows that the prewhitening algorithm can enhance the impulsive components of the signal. Therefore, the signals related to bearing faults can be preserved as much as possible along with the removal of other noises.

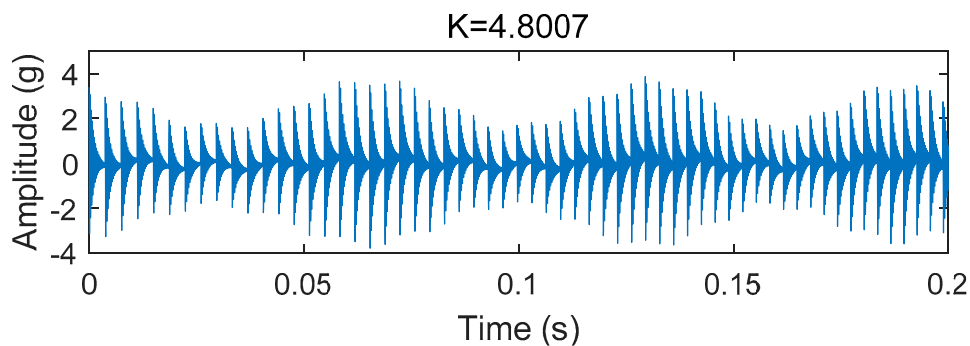


Figure 7. Pure simulation signal.

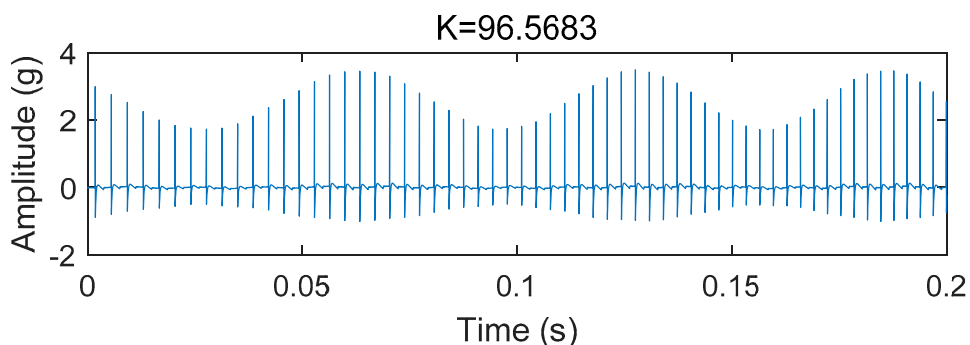


Figure 8. Result of simulation signal prewhitened by linear prediction.

For the fault signals obtained when intershaft bearings are used in practical applications in industry, the components are complex and the noises vary. Therefore, the benefits of using the prewhitening algorithm for the kurtosis may not be as obvious as shown above. However, this algorithm is very appropriate for extracting the fault features, which will be proven in Sections 5.6 and 5.7.

In order to prove the validity of the algorithm proposed in this paper, Gaussian noises are added to the fault simulation signals of the bearing operating at time-varying speeds, which leads the fault features of the bearing to be buried in noise. According to Equation (34) [15], the signal-to-noise ratio (SNR) is -22.52 dB.

$$SNR = 20 \log_{10}(P_s/A_n) \tag{34}$$

where P_s denotes the RMS value of the signal, A_n represents the peak value of the noise.

This makes the simulated signals more similar to those in the actual test. Figure 9 shows the signal without noises, and Figure 10 shows the signal after being affected by noises. Additionally, the corresponding speed trends are shown in Figure 11.

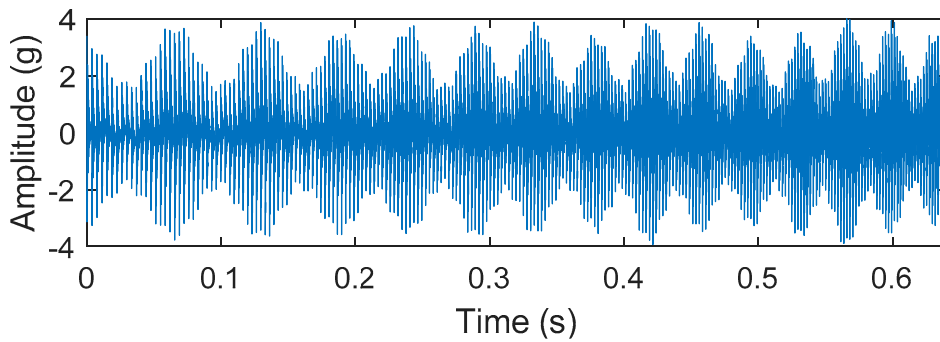


Figure 9. Simulated signal of bearing fault.

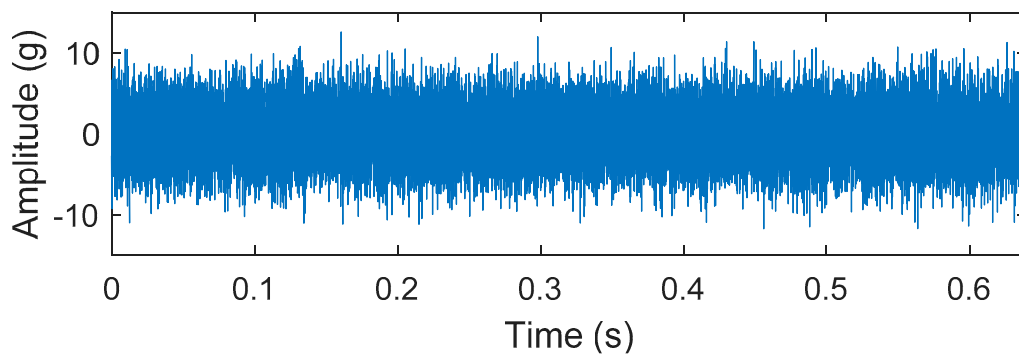


Figure 10. Simulated signal of bearing fault with noise.

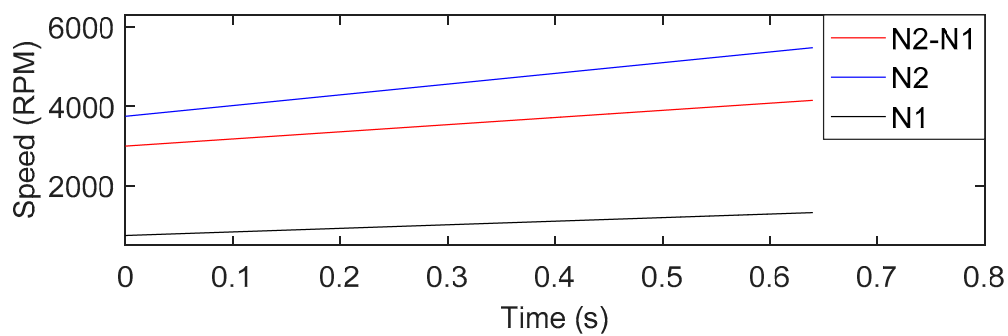


Figure 11. Simulated signal of speed trend.

As shown in Figure 12, the kurtogram is obtained after the algorithm is applied. The optimal demodulation center frequency is 4000 Hz, which is the same as the resonance frequency of the simulated signal. This proves that SK is highly significant.

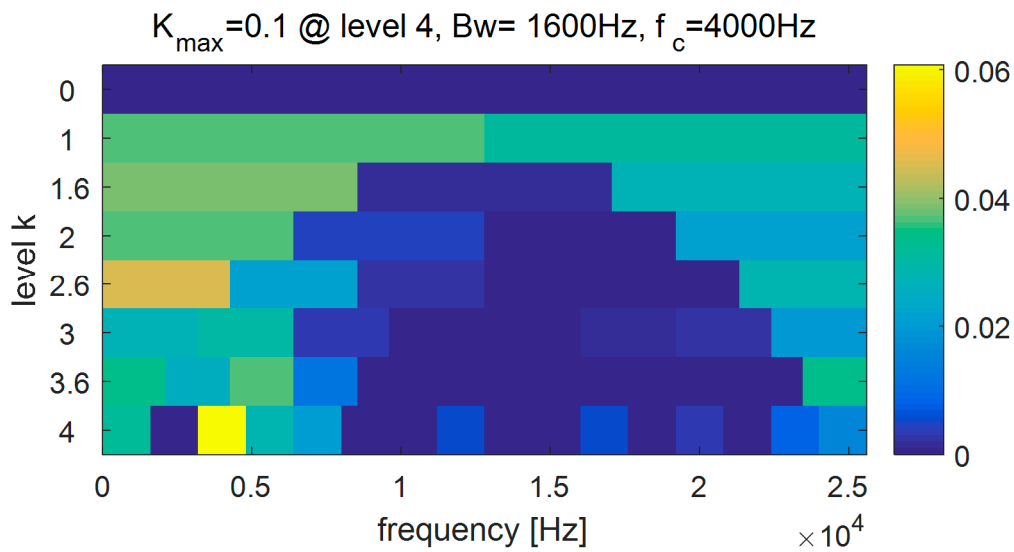


Figure 12. Kurtogram of noisy simulated signal.

Figure 13 shows the envelope order spectrum. The envelope spectrum is dominated by the orders 5.3 and 10.6, which are consistent with the FCF of the simulated signal. This spectrum proves that the proposed algorithm is very suitable for extracting weak fault features of intershaft bearings operating at variable speeds.

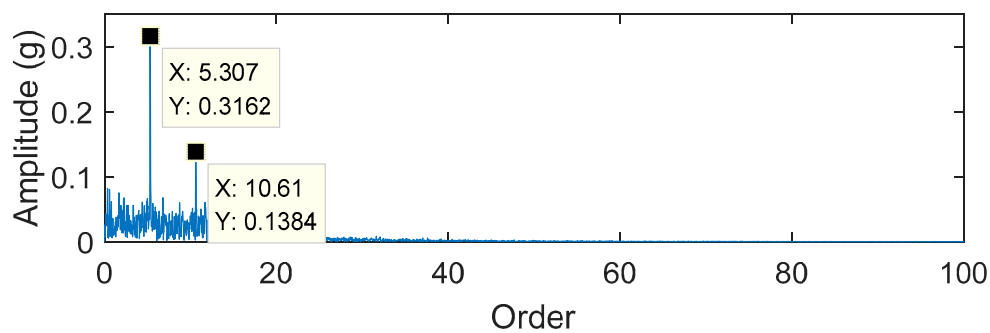


Figure 13. Envelope order spectrum of noisy simulated signal.

5. Experiments

This section examines the results of the fault simulations. A test bed for intershaft bearing was established. In this test bed, the speed difference of dual rotors, the bearing structure and its housing, and the mounting positions of the sensors were similar to those in a real gas turbine. Experiments were performed using the following steps: design and build a dual-rotor test bed; preset the faults of #1 intershaft bearing; and acquire the vibration signals from the #2 bearing housing.

5.1. Experimental Setup

The dual-rotor test bed was designed and built as shown in Figure 14.

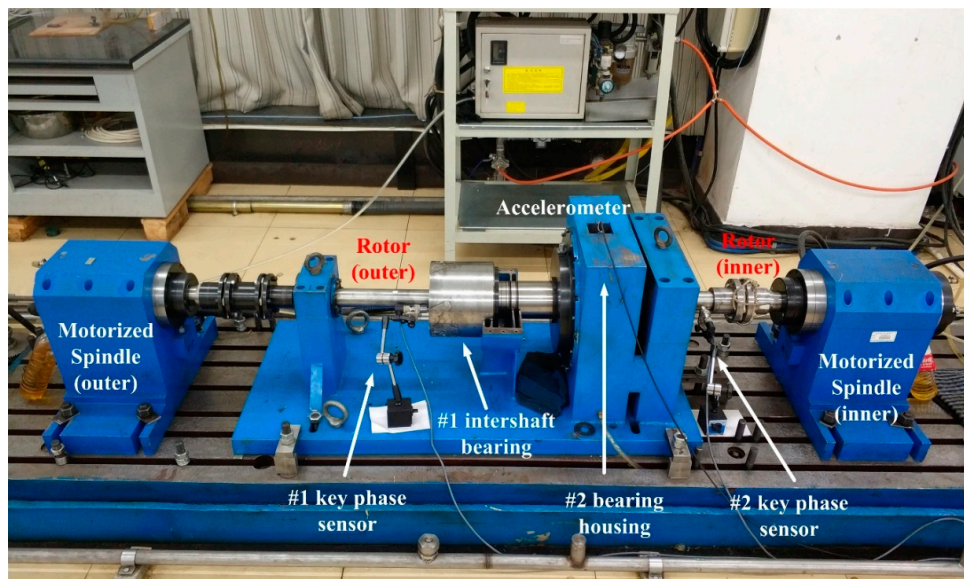


Figure 14. Dual-rotor vibration test bed.

The structure of the test bed includes the motorized spindle (outer rotor), coupling, bearing housing, #1 intershaft bearing, #2 bearing housing (including the bearing casing), bearing housing, coupling, and motorized spindle (inner rotor). To a large extent, the test bed reproduces the running status of an actual intershaft bearing and the sensor installation in the following three aspects.

- (1) In actual dual-rotor equipment, the intershaft bearing has no directly linked bearing housing. Therefore, the vibration response must be collected by indirect measurement. The vibration response of the intershaft bearing needs to be transferred to adjacent bearings via the shaft; then, via elastic supports and complicated thin-walled paths, the response is transferred to the sensor-equipped casing surface. As shown in Figure 15, the #2 bearing with a thin-walled casing as a support is the closest to the intershaft bearing on the test bed, which is similar to the structure of the actual dual-rotor equipment. The vibration of the #1 intershaft bearing is transferred to the #2 bearing via the rotor, which is in contact with the intershaft bearing. Then, the signal is transferred to the sensor position through the elastic support and the thin-walled struts of the #2 bearing. Finally, the signal can be detected. The transmission path in the test bed is almost the same as that in actual dual-rotor equipment.
- (2) In this test bed, the rotating speeds of the intershaft bearing's inner and outer rings are different and can vary frequently. The operating condition of the intershaft bearing in this test bed is similar to that in actual dual-rotor equipment.
- (3) The geometric parameters of the intershaft bearing used in the experiment are the same as those of the intershaft bearing in a certain dual-rotor gas turbine. The accelerometer is mounted on the #2 bearing housing, which is the closest to the intershaft bearing. As shown in Figures 14 and 15, the positions of the sensors (including the accelerometer and key phase sensors) are similar to those of the actual dual-rotor equipment.

The faults of inner and outer rings of the intershaft bearing were simulated as follows. As for the outer ring fault, a 1 mm deep and 1 mm wide groove was machined across the axis on the inner surface of the outer ring. As for the inner ring fault, a 1 mm deep and 1 mm wide groove was machined across the axis on the outer surface of the inner ring.

An LMS SCADAS data acquisition system was used [32], along with a BK4519 accelerometer as a vibration sensor, and a proximity switch as a key phase sensor. The accelerometer was installed in the vertical direction outside the thin-walled casing of the #2 bearing and controlled the rotational

speeds of the inner and outer rings via two motorized spindles. Finally, the fault data of the intershaft bearing at the variable rotational speeds of the inner and outer rings could be obtained.

The data used for analysis could be acquired from #2 bearing housing and consisted of two groups: (1) the fault data of the outer ring, where N_2 (rotational speed of outer ring) increased from 919 rpm to 1190 rpm, N_1 (rotational speed of inner ring) increased from 295 rpm to 395 rpm, the sampling frequency was 25.6 kHz, and the vibration waveform and speed trends are shown in Figure 16; (2) the fault data of the inner ring, where N_2 increased from 1743 rpm to 2237 rpm, N_1 increased from 418 rpm to 588 rpm, the sampling frequency was 102.4 kHz; the vibration waveform and speed trends are shown in Figure 17.

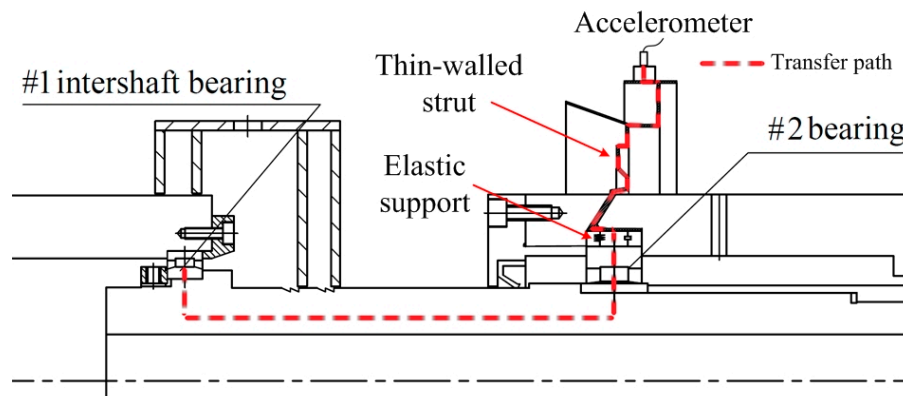


Figure 15. Transmission path of vibration signal of intershaft bearing.

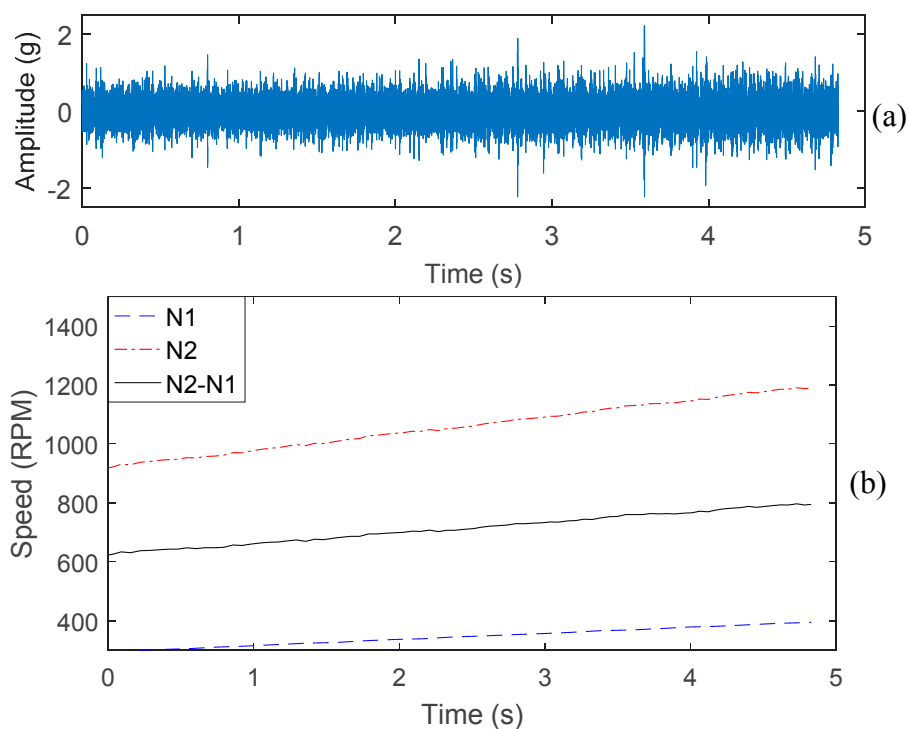


Figure 16. Fault in outer ring: (a) waveform of vibration and (b) speed trends.

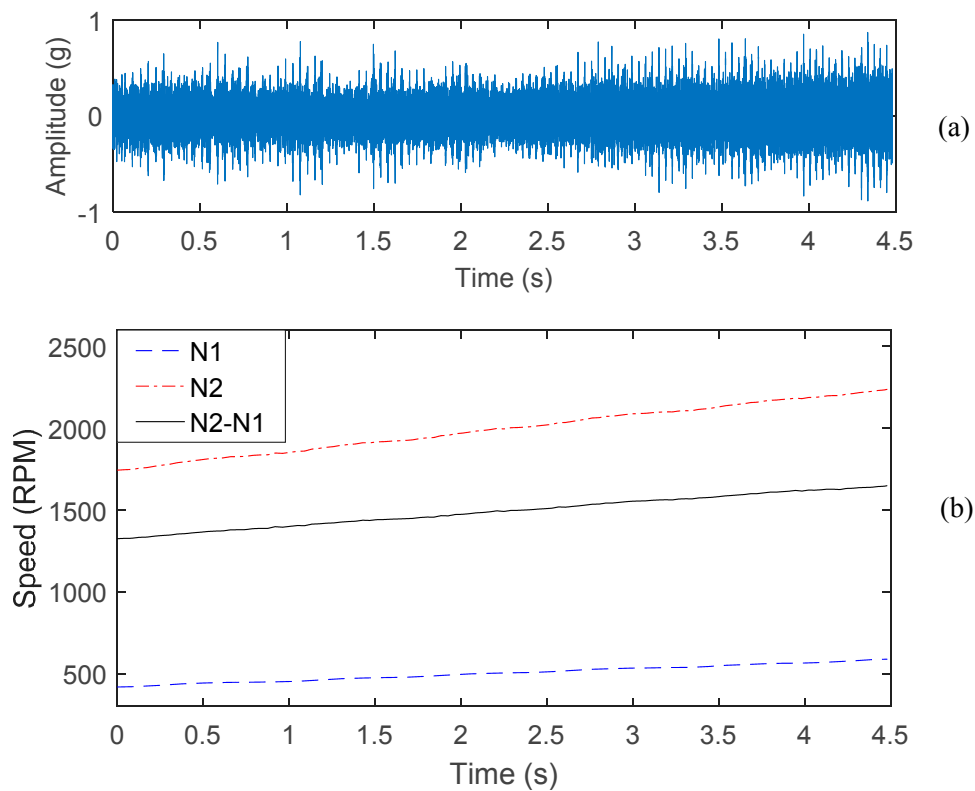


Figure 17. Fault in inner ring: (a) waveform of vibration and (b) speed trends.

5.2. FCFs of Intershaft Bearing

In the experiment, the intershaft bearing used was a uniserial roller bearing. The bearing parameters are listed in Table 1, and the bearing FCF orders are listed in Table 2.

Table 1. Geometric parameters of intershaft bearing.

Pitch Diameter D/mm	Ball Diameter d/mm	Contact Angle $\alpha/^\circ$	Number of Rolling Elements z
125	8	0	34

Table 2. Fault characteristic orders of intershaft bearing.

Outer Ring/Order	Inner Ring/Order	Rolling Elements/Order	Cage/Order
15.9	18.1	7.8	0.5

5.3. Diagnosis by Wavelet-Based Envelope Analysis

To show the advantages of the proposed method, the envelope demodulation method in the order domain, based on wavelet de-noising, is selected for comparison. The following steps can be used:

- (1) Order tracking. Even angle resampling in the speed difference domain, a method proposed in this paper, is applied to the original signal, achieving a stationary signal in the angle domain instead of a nonstationary signal in the time domain.
- (2) Signal decomposition and reconstruction with a wavelet packet are used to remove noises. “Sym8” (the wavelet packet basis function) and level 5 (the decomposition level) are selected to decompose and reconstruct signals in order to obtain the signal in the order domain after wavelet de-noising.
- (3) The envelope demodulation method based on the Hilbert transform is applied to achieving the envelope order spectrum.

The above envelope order demodulation algorithm can be applied to the fault data of the intershaft bearing, which are shown in Figures 16 and 17. Then, the envelope order spectrum is obtained, as shown in Figures 18 and 19.

Figure 18 shows the envelope order spectrum of the fault signal of the intershaft bearing's outer ring. In this spectrum, the highest amplitude order is 2.8, and is the result of other impacts in the rotor system and not the FCFs of the bearing. However, an order of 15.9, corresponding to a fault in the outer ring, is completely buried by noise.

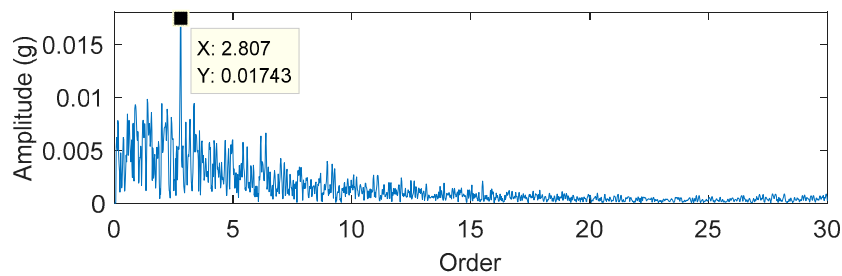


Figure 18. Envelope order spectrum of outer ring fault (envelope demodulation based on wavelet de-noising).

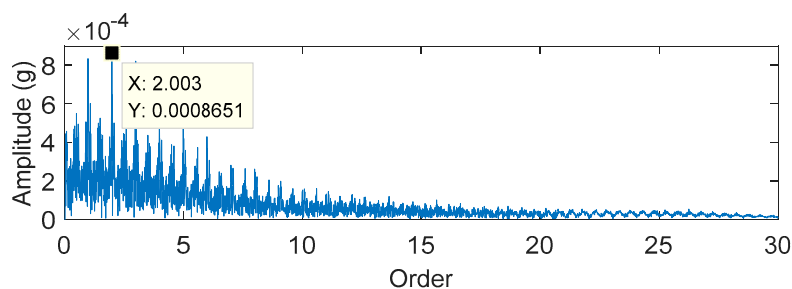


Figure 19. Envelope order spectrum of inner ring fault (envelope demodulation based on wavelet de-noising).

Figure 19 shows the envelope order spectrum of the fault signal of the intershaft bearing's inner ring. In this spectrum, the dominant order is 1 and its harmonics are caused by rotational speed differences in the inner and outer rings of the intershaft bearing. However, an order of 18.1, corresponding to the fault of the inner ring, is completely buried by noise.

The analysis results for the above two sets of data show that it is very difficult or even impossible for the envelope order demodulation algorithm to extract the weak fault features of intershaft bearing.

5.4. Diagnosis by VMD-Based Envelope Analysis

To show the superiority of the proposed method, the envelope demodulation method in the order domain, based on variational mode decomposition (VMD) is selected for comparison. The following steps can be used:

- (1) Order tracking. The same as (1) in Section 5.3.
- (2) Signal decomposition and reconstruction with VMD are used to remove noises [16], in order to obtain the signal in the order domain after de-noising.
- (3) The envelope demodulation method based on the Hilbert transform is applied to achieve the envelope order spectrum.

Then, the envelope order spectrum is obtained, as shown in Figures 20 and 21.

Figure 20 shows the envelope order spectrum of the fault signal of the intershaft bearing's outer ring. In this spectrum, the highest amplitude order is 1.2. An order of 15.9, corresponding to a fault in the outer ring, can be seen but it is not the dominant component.

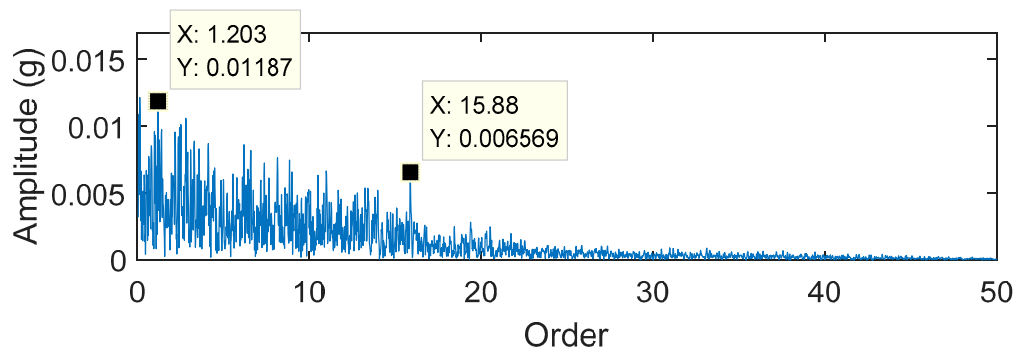


Figure 20. Envelope order spectrum of outer ring fault (envelope demodulation based on variational mode decomposition (VMD)).

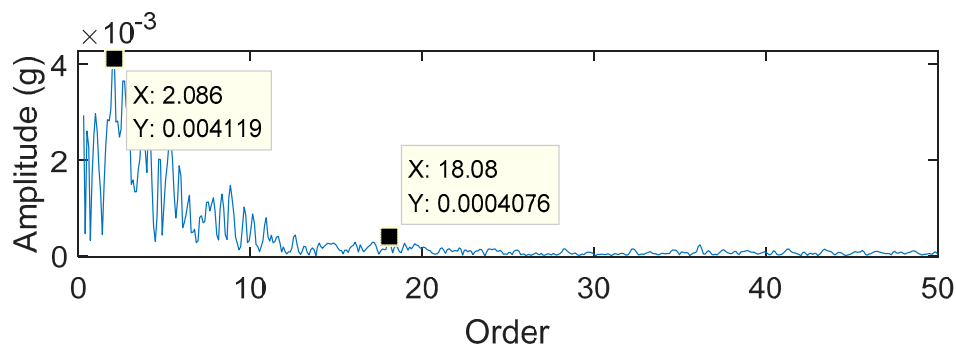


Figure 21. Envelope order spectrum of inner ring fault (envelope demodulation based on VMD).

Figure 21 shows the envelope order spectrum of the fault signal of the intershaft bearing's inner ring. In this spectrum, the dominant order is 2. An order of 18.1, corresponding to the fault of the inner ring, is completely buried by noise.

The analysis results for the above two sets of data show that it is very difficult or even impossible for the algorithm to extract the weak fault features of an intershaft bearing.

5.5. Diagnosis by Adaptive Filtering Based Envelope Analysis

To show the superiority of the proposed method, the envelope demodulation method in the order domain, based on adaptive filtering, is selected for comparison. The following steps can be used:

- (1) Adaptive filtering is adopted to reduce noise and harmonic components which are not the concerns in this research [33].
- (2) Order tracking. The same as (1) in Section 5.3.
- (3) The envelope demodulation method based on the Hilbert transform is applied to achieve the envelope order spectrum.

Then, the envelope order spectrum is obtained, as shown in Figures 22 and 23.

Figure 22 shows the envelope order spectrum of the fault signal of the intershaft bearing's outer ring. In this spectrum, the highest amplitude order is 2.7, and an order of 15.88 is the second high-amplitude component. An order of 15.88, corresponding to a fault in the outer ring, can be seen, but not the dominant component.

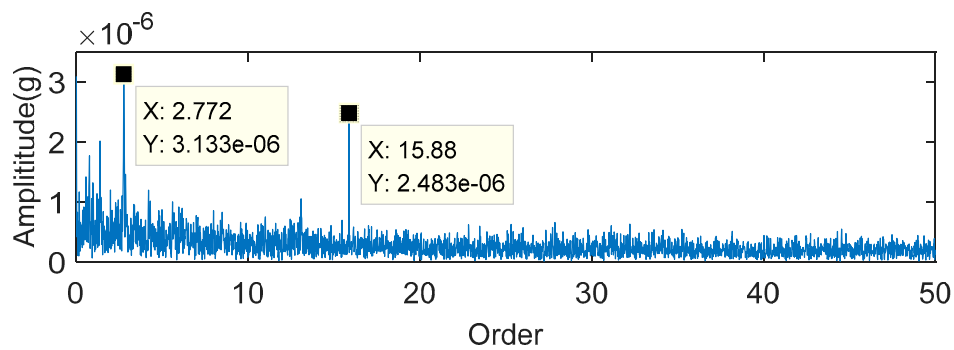


Figure 22. Envelope order spectrum of outer ring fault (envelope demodulation based on adaptive filtering).

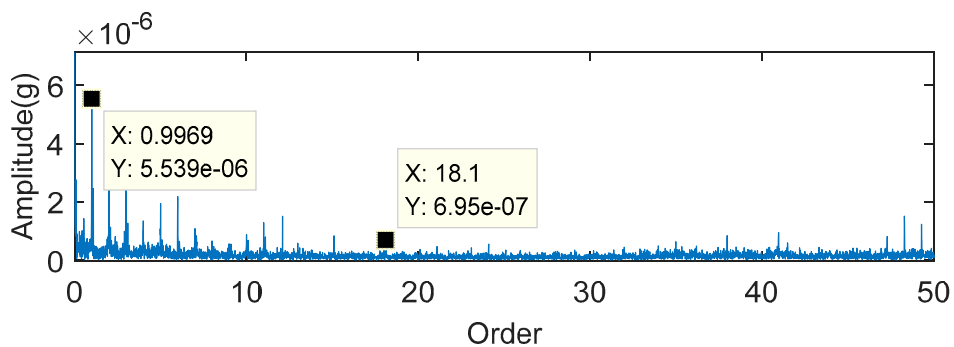


Figure 23. Envelope order spectrum of inner ring fault (envelope demodulation based on adaptive filtering).

Figure 23 shows the envelope order spectrum of the fault signal of the intershaft bearing's inner ring. In this spectrum, the dominant orders are 1 and its harmonics. An order of 18.1, corresponding to the fault of the inner ring, is completely buried by noise.

The analysis results for the above two sets of data show that it is very difficult for the algorithm to extract the weak fault features of intershaft bearing, especially that of the inner ring.

5.6. Diagnosis by SK-Based Envelope Analysis

In the three procedures of the proposed method in this paper, the prewhitening based on linear prediction is indispensable. If we removed this step, we could get the envelope order demodulation algorithm based on the SK. However, the following analysis shows that removing prewhitening is unacceptable.

Figure 24 shows the analysis results for the fault data of the intershaft bearing's outer ring using the envelope order demodulation algorithm based on SK. Figure 24a is the kurtogram. The SK shows that the center frequency of the optimum demodulation band is 2000 Hz, and the bandwidth is 800 Hz. In other words, the optimum demodulation band is [1600,2400] Hz. Figure 24b shows the envelope order spectrum. In this spectrum, an order of 2.8 is in the dominant position, which is almost the same as the results discussed in Section 5.3. An order of 15.9, corresponding to the fault in the bearing's outer ring, is not extracted.

Similarly, Figure 25 shows the analysis results for the fault data of the inner ring. Figure 25a shows the kurtogram. The SK shows that the center frequency of the optimum demodulation band is 12,800 Hz, and the bandwidth is 25,600 Hz. In other words, the optimum demodulation band is [0,25600] Hz. Figure 25b shows the envelope order spectrum. An order of 1 and its harmonic are the dominant components, which is similar to the results discussed in Section 5.3. An order of 18.1, corresponding to the fault of the bearing inner ring, is not extracted.

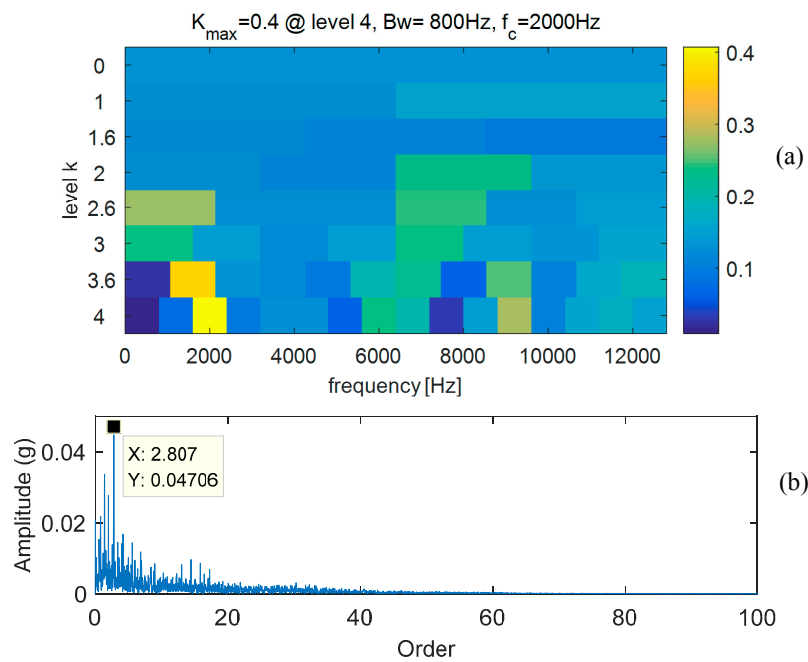


Figure 24. Analysis results for fault data of outer ring using envelope order demodulation algorithm based on spectral kurtosis (SK): (a) kurtogram and (b) envelope order spectrum.

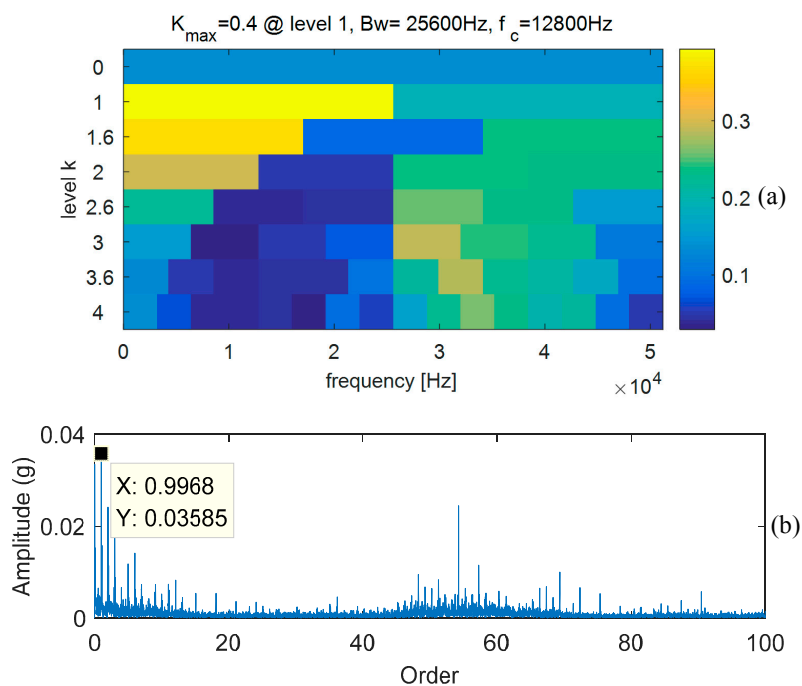


Figure 25. Analysis results for fault data of inner ring using envelope order demodulation algorithm based on SK: (a) kurtogram and (b) the envelope order spectrum.

The above analysis shows that the envelope order demodulation algorithm based on SK does not work well in extracting the weak fault features of the intershaft bearing.

5.7. Diagnosis by the Proposed Method

The proposed method was applied to the fault data of intershaft bearings, and the analysis results are shown in Figures 26 and 27.

Figure 26 shows the results for the fault data of the outer ring using the proposed method. Figure 26a is the kurtogram. The center frequency of the optimum demodulation band is 9200 Hz, and the bandwidth is 800 Hz. In other words, the optimum demodulation band is [8800,9600] Hz. Figure 26b shows the envelope order spectrum obtained by processing the data according to the demodulation bandwidth selected by (a). An order of 15.88 and its harmonic are the dominant components, which match the order of 15.9 for the FCFs of the intershaft bearing’s outer ring.

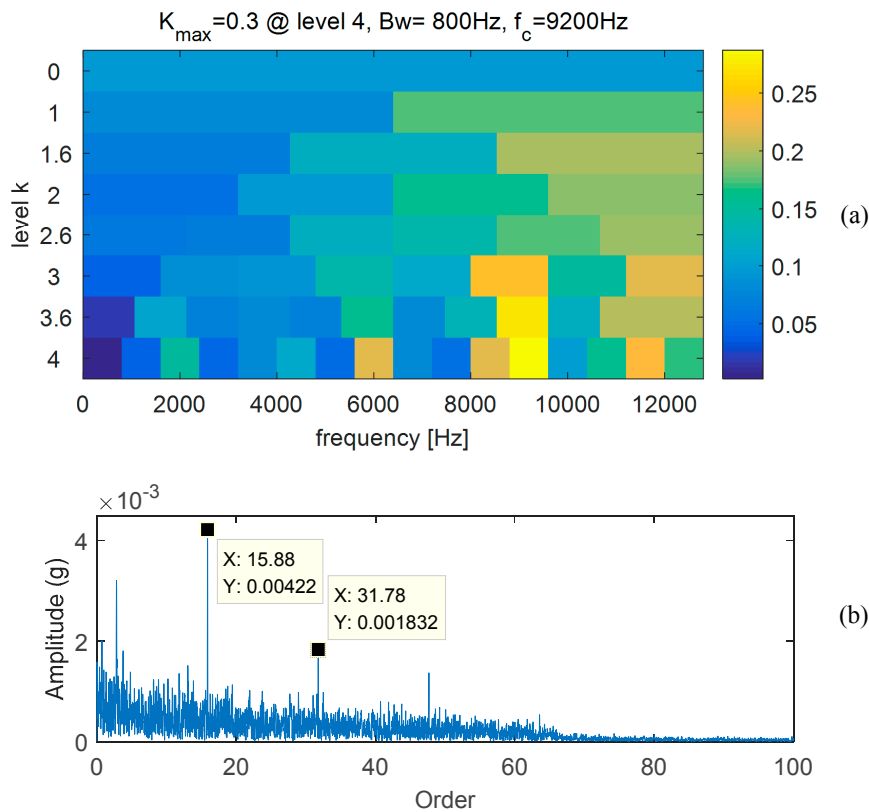


Figure 26. Analysis results for fault data of outer ring using algorithm proposed in this paper: (a) kurtogram and (b) envelope order spectrum.

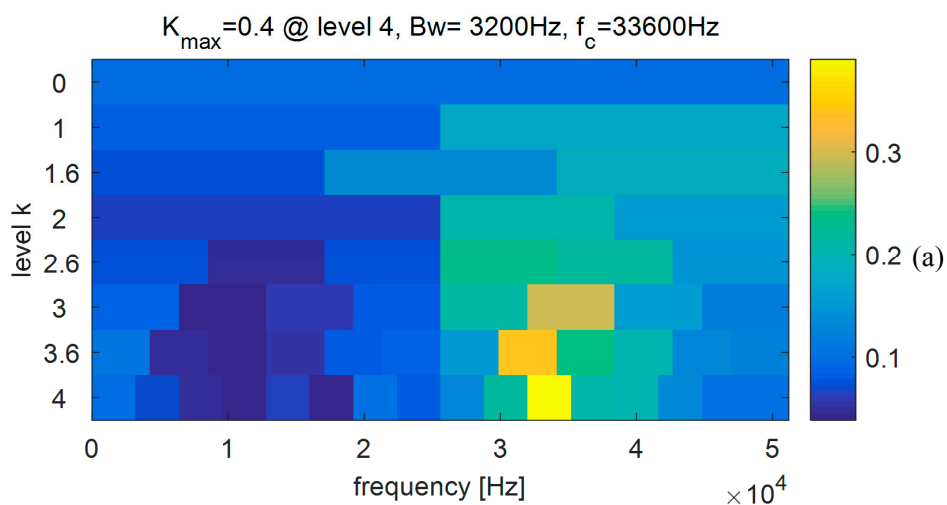


Figure 27. Cont.

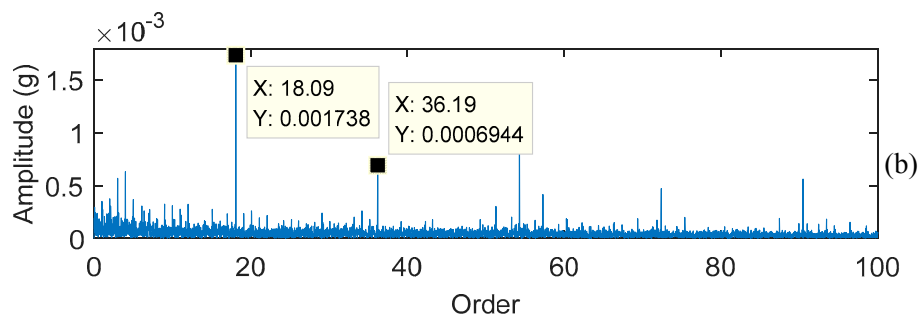


Figure 27. Analysis results for inner ring fault data using algorithm proposed in this paper: (a) kurtogram and (b) envelope order spectrum.

Similarly, Figure 27 shows the analysis results for the fault data of the inner ring. From Figure 27a, the center frequency of the optimum demodulation band is 33,600 Hz, and the bandwidth is 3200 Hz. In other words, the optimum demodulation band is [32000,35200] Hz. Figure 27b shows the envelope order spectrum. An order of 18.09 and its harmonic are the dominant components, which match the order of 18.1 for the FCFs of the intershaft bearing's inner ring.

The analysis of the experimental data shows that the proposed method is effective at extracting the weak fault features of intershaft bearings even in the presence of strong noises.

In addition, the demodulation bands in Sections 5.4 and 5.5 are completely different, leading to different calculation results. Compared with the algorithm in Section 5.5, the algorithm in Section 5.4 lacks the prewhitening step based on linear prediction. Prewhitening plays a key role in preprocessing the vibration signals of the intershaft bearing. This step retains the impulsive components of the bearing and filters out other noise components.

6. Conclusions

Both outer and inner rings of intershaft bearings rotate and the rotating speeds are different. The FCFs of intershaft bearings are relevant to the two speeds, so the calculation formulas of the FCFs of the intershaft bearings are different from those of traditional REBs. Calculation formulas for the FCFs of the intershaft bearings were obtained in this paper.

The order tracking method used in fault diagnosis for REBs only considers one rotating speed, so it is not applicable to intershaft bearings. Then, a correspondent order tracking method, order tracking in the rotating speed difference domain, was proposed in this research.

The feature extraction of the intershaft bearing's fault is more difficult than that of traditional REBs because the vibration signal of the intershaft bearings cannot be measured directly. The weak signal of the intershaft bearings is buried in strong vibration and interference as a result of indirect measurement. To solve this issue, a scheme based on linear prediction, SK, and order tracking in rotation speed difference domain is proposed to extract the weak fault features of intershaft bearings. A prewhitening method, based on linear prediction, is adopted to preprocess the fault data to remove stationary signals and preserve the nonstationary and impulsive signals. Optimal band-pass filter parameters were selected using the SK. The fault signal was also analyzed through the order tracking in the rotation speed difference domain when the bearings operate at variable speeds. The above three methods were combined in the proposed scheme. The simulated signals and experimental data were utilized to validate the effectiveness of the proposed scheme and the analysis results show that the proposed scheme can successfully extract the weak fault features of intershaft bearing.

7. Discussion

The proposed scheme can extract the fault features of intershaft bearings from indirectly measured signals and can be applied to fault diagnosis for gas turbines which have intershaft bearings. It can contribute to fault diagnosis for intershaft bearings and condition monitoring for gas turbines.

When the proposed scheme is implemented into real engineering equipment, the following aspects need to be carried out.

1. The accelerometer should be mounted in connecting flanges of the outer casing through sensor supports.
2. The sampling frequency should be high enough and it is better to achieve 100 kHz.
3. The rotating speeds of dual rotors should be collected as accurately as possible and it is better to utilize tooth-disc speed measurement.
4. Synchronous acquisition should be implemented between the vibration and the rotating speeds.

Acknowledgments: Support for this research was provided by the National Key Technologies R&D Program of China under grant No. 2016YFF0203305.

Author Contributions: Zhinong Jiang, Minghui Hu and Kun Feng conceived and designed the experiments; Minghui Hu and Kun Feng performed the experiments and collected the experimental signals; Minghui Hu and Ya He analyzed the data; Minghui Hu wrote the paper. Zhinong Jiang and Kun Feng reviewed and edited the manuscript.

Conflicts of Interest: The authors declare no conflict of interest.

References

1. Wei, X.; Feng, Y.; Yang, L.; Zhan, L. Research on fault prediction of main intershaft bearing of aircraft engine. In Proceedings of the Aviation Safety and Equipment Maintenance Technology Conference, Guangxi, China, 9–11 June 2014.
2. De Lacalle, L.N.L.; Viadero, F.; Hernández, J.M. Applications of dynamic measurements to structural reliability updating. *Probab. Eng. Mech.* **1996**, *11*, 97–105. [[CrossRef](#)]
3. Urbikain, G.; Olvera, D.; de Lacalle, L.N.L.; Elías-Zúñiga, A. Stability and vibrational behaviour in turning processes with low rotational speeds. *Int. J. Adv. Manuf. Technol.* **2015**, *80*, 871–885. [[CrossRef](#)]
4. Urbikain, G.; Campa, F.-J.; Zulaikab, J.-J.; de Lacalle, L.-N.; Alonso, M.-A.; Colladob, V. Preventing chatter vibrations in heavy-duty turning operations in large horizontal lathes. *J. Sound Vib.* **2015**, *340*, 317–330. [[CrossRef](#)]
5. Darlow, M.S.; Badgley, R.H. *Application of High Frequency Resonance Techniques for Bearing Diagnostics in Helicopter Gearboxes*; Technical Report; US Army Air Mobility Research and Development Laboratory: Cleveland, OH, USA, 1974; pp. 74–77.
6. Lv, F.; Cui, F.; Wang, X. Research on the wavelet de-noising of vibration signals for aircraft rolling bearings. *Mech. Res. Appl.* **2014**, *27*, 89–91.
7. Mishra, C.; Samantaray, A.K.; Chakraborty, G. Rolling element bearing defect diagnosis under variable speed operation through angle synchronous averaging of wavelet de-noised estimate. *Mech. Syst. Signal Process.* **2016**, *72–73*, 206–222. [[CrossRef](#)]
8. Dwyer, R.F. Detection of non-Gaussian signals by frequency domain kurtosis estimation. In Proceedings of the International Conference on Acoustics, Speech, and Signal Processing, Boston, MA, USA, 14–16 April 1983; pp. 607–610.
9. Antoni, J. The spectral kurtosis: A useful tool for characterising nonstationary signals. *Mech. Syst. Signal Process.* **2006**, *20*, 282–307. [[CrossRef](#)]
10. Antoni, J.; Randall, R.B. The spectral kurtosis: Application to the vibratory surveillance and diagnostics of rotating machines. *Mech. Syst. Signal Process.* **2006**, *20*, 308–331. [[CrossRef](#)]
11. Antoni, J. Fast computation of the kurtogram for the detection of transient faults. *Mech. Syst. Signal Process.* **2006**, *21*, 108–124. [[CrossRef](#)]
12. Sawalhi, N.; Randall, R.B. Spectral kurtosis optimization for rolling element bearings. In Proceedings of the ISSPA Conference, Sydney, Australia, 28–31 August 2005.

13. Wang, Y.; Liang, M. Identification of multiple transient faults based on the adaptive spectral kurtosis method. *J. Sound Vib.* **2012**, *331*, 470–486. [[CrossRef](#)]
14. Wang, Y.; Xiang, J.; Market, R. Spectral kurtosis for fault detection, diagnosis and prognostics of rotating machines: A review with application. *Mech. Syst. Signal Process.* **2016**, *66–67*, 679–698. [[CrossRef](#)]
15. Tian, X.; Gu, J.X.; Rehaba, I.; Abdallaa, G.M.; Gu, F.; Balla, A.D. A robust detector for rolling element bearing condition monitoring based on the modulation signal bispectrum and its performance evaluation against the Kurtogram. *Mech. Syst. Signal Process.* **2018**, *100*, 167–187. [[CrossRef](#)]
16. Zhang, M.; Jiang, Z.; Feng, K. Research on variational mode decomposition in rolling bearings fault diagnosis of the multistage centrifugal pump. *Mech. Syst. Signal Process.* **2017**, *93*, 460–493. [[CrossRef](#)]
17. Potter, R. A New Order Tracking Method for Rotating Machinery. *Sound Vib.* **1990**, *24*, 30–34.
18. Fyfe, K.R.; Munck, E.D.S. Analysis of computed order tracking. *Mech. Syst. Signal Process.* **1997**, *11*, 187–205. [[CrossRef](#)]
19. Borghesani, P.; Ricci, R.; Chatterton, S. A new procedure for using envelope analysis for rolling element bearing diagnostics in variable operating conditions. *Mech. Syst. Signal Process.* **2013**, *38*, 23–35. [[CrossRef](#)]
20. Randall, R.B. *Vibration-Based Condition Monitoring: Industrial, Aerospace and Automotive Applications*; John Wiley and Sons: West Sussex, UK, 2011; pp. 207–214. ISBN 978-0-470-74785-8.
21. Sawalhi, N. *Diagnostics, Prognostics and Fault Simulation for Rolling Element Bearings*. Ph.D. Thesis, The University of New South Wales, Randwick City, Australia, April 2007.
22. Guo, Y.; Liu, T.-W.; Na, J. Envelope order tracking for fault detection in rolling element bearings. *J. Sound Vib.* **2012**, *331*, 5644–5654. [[CrossRef](#)]
23. Mcfadden, P.D.; Smith, J.D. The vibration produced by multiple point defects in a rolling element bearing. *J. Sound Vib.* **1985**, *98*, 263–273. [[CrossRef](#)]
24. Randall, R.B.; Antoni, J. Rolling element bearing diagnostics—A tutorial. *Mech. Syst. Signal Process.* **2011**, *25*, 485–520. [[CrossRef](#)]
25. Shi, L.; Shen, J.; Zhang, Y. Fault diagnosis of a rolling element bearing based on AR model and spectral kurtosis. *J. Vib. Shock* **2011**, *30*, 257–260.
26. Xing, W.; Niu, J. Power spectrum estimation based on AR model. *Mod. Electron. Technol.* **2011**, *34*, 49–51.
27. Vold, H.; Leuridan, J. High resolution order tracking at extreme slew rates using Kalman tracking filters. *Shock Vib.* **1995**, *2*, 507–515. [[CrossRef](#)]
28. Bai, M.; Huang, J.; Hong, M. Fault diagnosis of rotating machinery using an intelligent order tracking system. *J. Sound Vib.* **2005**, *280*, 699–718. [[CrossRef](#)]
29. Randall, R.B.; Antoni, J. The relation between spectral correlation and envelope analysis in the diagnostics of bearing faults and other cyclostationary machine signals. *Mech. Syst. Signal Process.* **2001**, *15*, 945–962. [[CrossRef](#)]
30. Antoni, J.; Raad, A. Cyclostationary modelling of rotating machine vibration signals. *Mech. Syst. Signal Process.* **2004**, *18*, 1285–1314. [[CrossRef](#)]
31. Cong, F.; Chen, J.; Dong, J.; Pecht, M. Vibration model of rolling element bearings in a rotor-bearing system for fault diagnosis. *J. Sound Vib.* **2013**, *332*, 2081–2097. [[CrossRef](#)]
32. Siemens, LMS SCADAS [EB/OL]. Available online: <https://www.plm.automation.siemens.com/zh/products/lms/testing/scadas/lab.shtml> (accessed on 15 July 2017).
33. Islam, M.S.; Cho, S.; Chong, U. Bearing fault detection and identification using adaptive filter and computed order tracking. In Proceedings of the IEEE International Conference on Informatics, Electronics and Vision, Dhaka, Bangladesh, 13–14 May 2016.

